

Submitted: ApJ, March 03, 2013; Revised: August 09, 2013

A Preliminary Calibration of the RR Lyrae Period-Luminosity Relation at Mid-Infrared Wavelengths: WISE Data

Barry F. Madore

*Observatories of the Carnegie Institution of Washington
813 Santa Barbara St., Pasadena, CA 91101*

Douglas Hoffman

*Infrared Processing and Analysis Center
770 South Wilson, Pasadena, CA 91125*

Wendy L. Freedman, Juna A. Kollmeier, Andy Monson

S. Eric Persson, Jeff A. Rich Jr., Victoria Scowcroft, Mark Seibert

*Observatories of the Carnegie Institution of Washington
813 Santa Barbara St., Pasadena, CA 91101*

barry@obs.carnegiescience.edu, dhoffman@ipac.caltech.edu
wendy@obs.carnegiescience.edu, jak@obs.carnegiescience.edu
amonson@obs.carnegiescience.edu, persson@obs.carnegiescience.edu
jrich@obs.carnegiescience.edu, vs@obs.carnegiescience.edu,
mseibert@obs.carnegiescience.edu

ABSTRACT

Using time-resolved, mid-infrared data from WISE and geometric parallaxes from *HST* for four Galactic RR Lyrae variables, we derive the following Population II Period-Luminosity (PL) relations for the WISE[W1], [W2] and [W3] bands at 3.4, 4.6 & 12 μm , respectively:

$$M_{[W1]} = -2.44 (\pm 0.95) \times \log(P) - 1.26 (\pm 0.25) \quad \sigma = 0.10$$

$$M_{[W2]} = -2.55 (\pm 0.89) \times \log(P) - 1.29 (\pm 0.23) \quad \sigma = 0.10$$

$$M_{[W3]} = -2.58 (\pm 0.97) \times \log(P) - 1.32 (\pm 0.25) \quad \sigma = 0.10$$

The slopes and the scatter around the fits are consistent with a smooth extrapolation of those same quantities from previously-published K-band observations at 2.2 μm , where the asymptotic (long-wavelength) behavior is consistent with a Period-Radius relation having a slope of 0.5. No obvious correlation with metallicity (spanning 0.4 dex in [Fe/H]) is found in the residuals of the four calibrating RR Lyrae stars about the mean PL regression line.

Subject headings: Stars: Variables: RR Lyrae stars– Stars: Variables: W Virginis stars

1. Introduction

The advantages of moving the Population I calibration of the Classical Cepheid Period-Luminosity relation (the Leavitt Law) from the optical to the infrared were outlined some three decades ago by McGonegal et al. (1983), and they have been borne out repeatedly over the years, as reviewed and elaborated upon by Freedman & Madore (2010). But only now is it possible to extend these same advantages to the parallel path offered by the Population II variable stars (the short-period RR Lyrae variables and their longer-period siblings the W Virginis stars). Two impressive accomplishments have made this possible: (1) the completion of the WISE mission (Wright et al. 2010) and the release of its sky survey of point sources measured in the mid-infrared in four bands ranging from 3.4 to 22 μm , and then (2) the innovative application of the *HST* Fine-Guidance Sensor (*FGS*) cameras to the

determination of trigonometric parallaxes to four field RR Lyrae variables by Benedict et al. (2011).

The many, now well-known, advantages of calibrating and using period-luminosity relations in the mid-IR include the following: (1) the effects of line-of-sight extinction are reduced with respect to optical observations by at least an order of magnitude for even the shortest wavelength ([W1] at $3.4 \mu\text{m}$) observations, (2) concerns about the systematic impact of the possible non-universality of the reddening law are similarly reduced by going away from the optical and into the mid-IR, (3) the total amplitude of the light variation of the target star during its pulsation cycle is greatly reduced because of the largely diminished contribution of temperature variation to the change in surface brightness, in comparison to the much smaller (but essentially irreducible) wavelength-independent radius/areal variations, (4) the corresponding collapse in the width (i.e., intrinsic scatter) of the period-luminosity relations, again because of the reduced sensitivity of infrared luminosities to temperature variations (across the instability strip), combined with the intrinsic narrowness of the residual period-radius relations. And finally, (5) at mid-infrared wavelengths, for the temperatures and surface gravities encountered in Population I & II Cepheids and RR Lyrae stars, there are so few metallic line or molecular transitions in those parts of the spectrum that atmospheric metallicity effects are expected to have minimal impact on the calibration.¹ This is especially true for the RR Lyrae stars which are significantly hotter than their longer-period (cooler) Cepheid counterparts.

As described in Freedman et al. (2012), the *Carnegie Hubble Program* (CHP) is designed to minimize and/or eliminate the remaining known systematics in the measurement of the Hubble constant using mid-infrared data from NASA’s *Spitzer Space Telescope*. Here we broaden the base in two distinct ways: (a) the incorporation of WISE mid-infrared data and (b) the preliminary calibration of the Population II RR Lyrae variables as mid-infrared distance indicators. This new initiative is known as the *Carnegie RR Lyrae Program* (CRRP).

¹One significant exception at $4.5 \mu\text{m}$ has been noted for long-period Cepheids, where a CO molecular bandhead appears at temperatures below 4000K; see Marengo et al. 2010, Scowcroft et al. 2011, and Monson et al. 2012; however, the temperatures of the RR Lyrae variables, are so high in comparison to the long-period (classical) Cepheids, where this effect was discovered, that we expect no contribution of CO to the light or color curves of the RR Lyrae variables studied here. The W Virginis stars may be affected, and still need to be examined.

2. The Calibrators: WISE Observations

WISE conducted an all-sky survey at four mid-infrared wavelengths, 3.4, 4.6, 12 and 22 μm (W1, W2, W3 and W4, hereafter). As such all of the RR Lyrae variables having trigonometric parallaxes (Benedict et al. 2011) were also observed by the satellite. By design, the slowly precessing orbit of WISE, allowed the satellite to scan across every object on the sky at least 12 times (with progressively more coverage at higher ecliptic latitudes). These successive observations were obtained within a relatively narrow window of time (over about 18 hours for those fields nearest the ecliptic equator) with each observation being separated by about 90 minutes (the orbital period of the satellite). Fortunately RR Lyrae stars have periods that are generally less than 16 hours, meaning that even the sparsest of these multiple mid-infrared observations covered at least one full pulsational cycle of these particular variable stars.

The light curves based on the time-resolved WISE observations of our calibrating stars are shown in Figures 1 & 2 for the four RR Lyrae variables, *SU Dra*, *RR Lyr*, *XZ Cyg*, & *UV Oct*. These stars were observed by WISE 51, 23, 24 and 23 times, respectively. Data were retrieved from the WISE All-Sky Single Exposure (L1b) Source Table, which is available at the Infrared Science Archive (<http://irsa.ipac.caltech.edu/Missions/wise.html>). The source positions were queried with a 2.5 arcsec cone search radius, ignoring observations flagged as contaminated by artifacts. The observations are very uniformly distributed around the cycle and the resulting light curves are exceedingly well defined. All three of the shortest-wavelength light curves show convergence in their properties, exemplified by their mutual phases, shapes and amplitudes². As expected these light curves closely track the anticipated light variations due to surface-area variations of the star, where at these wavelengths the sensitivity of the surface brightness to a temperature variation is much diminished as compared to its sensitivity at optical wavelengths. This then fully accounts for the mutual phasing (tracking the radius variations, and not the off-set temperature variations), the shape (the cycloid-like radius variation, in contrast to the highly asymmetric color/temperature variation) and the low amplitude (around 0.3 mag, peak-to-peak, in line with the small, radius-induced cyclical change in surface area of these stars).

The non-parametric fitting methodology, GLOESS was used to derive intensity-averaged magnitudes and amplitudes, as given in Table 1 (see Persson et al. 2004 for a description

²It should be noted that RR Lyr is saturated in the WISE data, and there is a documented flux over-estimation bias for saturated sources, especially in W2 (Cutri et al. 2012). However, we have made no correction for the bias as it only becomes detectable for sources brighter than 4.0 mag for W1 and 6.0 mag for W2.

and an early application of this fitting technique).

3. RR Lyrae Period-Luminosity Relations

Table 1 contains the parameters needed to compute absolute mean magnitudes. The parallaxes, E(B-V) reddenings, and Lutz-Kelker-Hanson (LKH; Lutz and Kelker 1973; Hanson 1979) corrections as taken from Benedict et al 2011, are listed for convenience. We have converted the A_V extinctions listed by Benedict et al. (2011) to those in the W1 and W2 bands using the Yuan et al. (2011) compilation of $A_{WISE}/E(B-V)$ results with $A_V/E(B-V) = 3.1$. Indebetouw et al. (2005) give values of $A_{Spitzer}/A_K^3$, which we converted to A_{WISE}/A_V via the Cardelli et al.(1989) law. The values of A_{WISE}/A_V given by Yuan et al. (2011) and our pseudo-values from Indebetouw et al. (2005) agree well. Neither the Yuan et al. (2011) nor Indebetouw et al. (2005) results extend to the W3 band, and here we have referred to Fitzpatrick (1999) for an approximate value. The extinctions for the four stars are so small as to make no difference to the absolute magnitude values and we take A_{W3}/A_V to be 0.01. The adopted mid-IR extinctions A_{WISE}/A_V we adopt are 0.065, 0.052, and 0.01 for W1, W2, and W3, respectively. The adopted mid-IR extinctions $A_{WISE}/E(B-V)$ are also given in Table 1. The above parameters and our observed mean magnitudes lead to the W1, W2, and W3 absolute magnitudes in Table 1⁴. and the Period-Luminosity relations for RR Lyrae variables follow:

$$M_{[W1]} = -2.44 (\pm 0.95) \times \log(P) - 1.26 (\pm 0.25) \quad \sigma = 0.10$$

$$M_{[W2]} = -2.55 (\pm 0.89) \times \log(P) - 1.29 (\pm 0.23) \quad \sigma = 0.10$$

$$M_{[W3]} = -2.58 (\pm 0.97) \times \log(P) - 1.32 (\pm 0.25) \quad \sigma = 0.10$$

The absolute magnitude values and the respective fits to the first two WISE bands and as well as K-band data (from Benedict et al. 2011 and Dall’Ora et al. 2004, respectively) are shown in Figure 3. Despite the very small (less than a factor of two) range in period covered by RR Lyrae stars, the PL relations are well defined, largely because of their intrinsically small scatter. The intrinsic scatter is especially well illustrated by the K-band PL relation,

³The Indebetouw et al. values, strictly speaking, actually apply to the Spitzer channels 1 and 2 bands which are quite close to the W1 and W2 bands; the differences can be safely ignored.

⁴Our magnitudes differ slightly from those in Benedict et. (2011). These differences stem from our use of different reddening law assumptions together with typographical errors in their Table 8 (Benedict 2013, private communication).

where we also show the RR Lyrae data of Dall’Ora et al. for 21 fundamental-mode RR Lyrae stars in the well-populated LMC globular cluster, Reticulum (shifted by 18.47 mag). A comparison of these two datasets is very illuminating. The slope of the adopted PL relation at K and the total width of it, as defined by the two samples, are for all intents and purposes, identical. The very good agreement in these two independently-determined slopes and the small dispersion in each of the datasets suggest that the means of the Milky Way variables are already well constrained even though the Galactic calibrating sample itself is currently very small.

On the other hand, we note that the small (observed) scatter of the Milky Way RR Lyrae variables around each of the adopted PL relations is apparently at variance with the individually quoted error bars for each of the calibrating variables. That is, the formal scatter of ± 0.10 mag in the WISE PL relations is to be compared with the quoted parallax errors on the individual distance moduli of ± 0.22 , ± 0.16 , ± 0.25 and ± 0.07 mag for XZ Cyg, UV Oct, SU Dra and RR Lyr, respectively. The average scatter for the variables (± 0.18 mag) is then about two times larger than their observed scatter around the PL fit. This suggests that the published errors may be somewhat overestimated. There are independent data that support this assertion. The 10 Galactic Cepheids for which Benedict et al. (2010) obtained parallaxes, using the same instrument, telescope and reduction methodology have individually quoted internal errors in their true distance moduli ranging from ± 0.11 to ± 0.30 mag. Their average uncertainty is ± 0.19 mag, and yet, once again, as with the RR Lyrae variables the PL fit to these data yields a formal dispersion of only ± 0.10 mag. In both cases the observed dispersions, for the Galactic samples, are in total agreement with independently determined dispersions for the much more robustly determined dispersions for the LMC samples. We suggest therefore that the random errors reported for the *HST* parallaxes for both the Cepheids and for the RR Lyrae variables may have been over-estimated. This is not simply of academic interest. If the observed scatter is used to calculate the systematic uncertainty in the calibration of the RR Lyrae PL relation that uncertainty would be $0.10/\sqrt{4} = \pm 0.05$ mag, a 2-3% error in the Population II distance scale. However, if the quoted errors on the individual distance moduli are used, then the uncertainty rises to $0.18/\sqrt{4} = \pm 0.09$ mag, a 5% error. Similar conclusions would also apply to the base uncertainty in the Cepheid distance scale using the Benedict sample; is the uncertainty in the Galactic Cepheid zero point 1.6% in distance, or is it 3.0%? It is therefore important to note that in their first paper discussing the use of *FGS* on *HST*, Benedict et al. (2002) state that the “standard deviations of the *HST* and *Hipparcos* data points may have been overstated by a factor of ~ 1.5 .” and since the *Hipparcos* errors had been subjected to many confirming tests “... that it is likely that the *HST* errors are overstated.” Parallaxes from Gaia are anxiously awaited; they will improve the number of calibrators by orders of magnitude and convincingly set the zero point.

In Figure 3 we show, using thick vertical lines, the full magnitude of the LKH corrections as published by Benedict et al (2011) and applied to the true distance moduli used here. It is noteworthy that, if these corrections had not been applied, the dispersion in the data points around the fit would have exceeded the independently determined dispersion from the Reticulum data, and the slope of the Milky Way solution would have been more shallow than the LMC slope. We take the final agreement of both the slopes and the dispersions to suggest that the individually determined and independently-applied LKH corrections are appropriate.

Finally, it needs to be noted that Klein et al. (2011) have published slopes that are much shallower than the ones derived here (e.g., -1.7 compared to our -2.6). This is because in their Bayesian analysis they chose to leave the overtone pulsators in the global solution, without correcting them to their equivalent fundamental periods. We have recomputed the slopes from their data after applying the appropriate period shift to the overtones, and those PL slopes are plotted in Figure 4. Their slopes and ours now agree well within the errors, but they are still systematically somewhat shallower than our solutions.

4. The Run of PL Slope with Wavelength

For Cepheids it is well known that the slope of the PL relation is a monotonically increasing function of wavelength. In Figure 4 we show that the same overall trend is now made explicit for the first time for the RR Lyrae variables as well, and for the same physical reasons. As one moves from shorter to longer wavelengths one is moving from PL relations where the slope is dominated by the trend of decreasing temperature (i.e., decreasing surface brightness) with period, to relations that are dominated by the opposing run of increasing mean radius with period. The plotted slopes of the optical and near-infrared PL relations are representative of a variety of published studies (e.g, Catelan, Pritzl & Smith 2004, Benedict et al. 2011, Dall’Ora et al. 2004) while the mid-IR slopes are from this study. As the relative contribution from the temperature-sensitive surface brightness drops off with wavelength, the observed slope is expected to asymptotically approach the wavelength-independent (geometric) slope of the Period-Area relation. That behavior is indeed seen in Figure 4. Moreover the level at which the plateau is occurring would suggest that the period-radius relation of Burki & Meylan (1986) (giving a slope of -2.60, based on Baade-Wesselink studies) is marginally preferred over the period-radius (slope = -3.25) and

period-radius-metallicity (slope = -2.90) solutions given by Marconi et al. (2005)⁵

From a practical point of view it is not immediately clear what advantage the increased slope of the long-wavelength PL relations would have to offer applications to the distance scale, until it is realized that increased slope in the PL relation is causally and physically connected to decreased width (i.e., decreased intrinsic scatter and therefore increased precision) in the PL relation as proven in the general case by Madore & Freedman (2012). This effect can be seen for the RR Lyrae variables in Figure 2 of Catelan, Pritzl & Smith (2004), and it is apparent here in Figure 3 where the scatter has already reached a minimum in the K-band where simultaneously the plateau in slope (seen in Figure 4) is very nearly complete.

5. A First Test of the Metallicity Dependence in the Mid-IR

In Figure 5 we plot the measured magnitude residuals from the [W1] 3.4 μm PL relation versus the published metallicities of the four RR Lyrae stars in our sample, as given in Table 1 of Benedict et al. (2011). The RR Lyrae stars only sample a 0.4 dex range in [Fe/H] so the test is not a strong one, but there is clearly no significant dependence of the already small magnitude residuals on metallicity.

6. Conclusions

As can be dramatically seen in the study of Catelan, Pritzl & Smith (2008, especially their Figure 2) operating anywhere in the near to mid-infrared, from $H = 1.6 \mu\text{m}$ (accessible to *HST*) to 3.6 μm (accessible to Spitzer now, and with JWST in the near future) will each accrue the benefits of low scatter and ever decreasing sensitivity (with wavelength) to line-of-sight extinction. Collecting power, availability and spatial resolution will determine which of these instruments will be used at any given time. But suffice it to say that the Population II RR Lyrae variables are proving themselves to be a powerful means of establishing an independent, highly precise and accurate distance scale that is completely decoupled in its systematics from the Population I Cepheid path to the extragalactic distance scale and

⁵The referee has correctly pointed out that “the Period-Radius relation provided by Burki & Meylan (1986) is based on a mix of δ Scuti, RR Lyrae and Type II (W Virginis) stars”, and that “there is no solid reason why the quoted pulsators should obey the same PR relation.” At the same time, he/she notes that “the Period-Radius relation provided by Marconi et al. (2005) is based on a set of RR Lyrae models that cover more than two dex in metal abundance ... and they also account for, at fixed metal abundance, possible evolutionary effects.”

the Hubble constant.

This work is based in part on observations made with the *Wide-field Infrared Survey Explorer* (WISE), which is operated by the Jet Propulsion Laboratory, California Institute of Technology under a contract with NASA. Support for this work was provided by NASA through an award issued by JPL/Caltech. This research also made use of the NASA/IPAC Extragalactic Database (NED) and the NASA/IPAC Infrared Science Archive (IRSA), both of which are operated by the Jet Propulsion Laboratory, California Institute of Technology, under contract with the National Aeronautics and Space Administration. We thank Fritz Benedict for numerous frank and useful communications. The referee was especially helpful in bringing this paper to a more correct and fruitful completion.

References

- Benedict, G. F., McArthur, B.E., Feast, M.W., et al. 2011, *AJ*, 142, 187
- Benedict, G. F., McArthur, B.E., Fredrick, L.W., et al. 2002, *AJ*, 124, 1695
- Burki, G., & Meylan, G. 1986, *A&A*, 159, 261
- Cardelli, J.A., Clayton, G.C., & Mathis, J.S 1989, *ApJ*, 345, 245
- Catelan, M., Pritzl, B.J., & Smith, H.A. 2004, *ApJS*, 154, 633
- Cutri et al. 2012, WISE All-Sky Release Explanatory Supplement,
<http://wise2.ipac.caltech.edu/docs/release/allsky/expsup/>
- Dall’Ora, M., Storm, J., Bono, G., et al. 2004, *ApJ*, 610, 269
- Fitzpatrick, E.L. 1999, *PASP*, 111, 63
- Freedman, W.L., & Madore, B.F. 2010, *ARA&A*, 48, 673
- Indebetouw, R., Mathis, J. S., & Babler, B. L. et al. 2005, *ApJ*, 619, 931
- Klein, C.R., Richards, J.W., Butler, N.R., & Bloom, J.S. 2011, *ApJ*, 738, 185
- Madore, B.F. & Freedman, W.L. 2010, *ApJ*, 744, 132
- Marconi, M., Nordgren, T., Bono, G., Schnider, G., & Caputo, F. 2005, *ApJ*, 623, 133
- McGonegal, R., McAlary, C.W., McLaren, R.A. & Madore, B.F. 1983, *ApJ*, 257, 33
- Marengo, M., Evans, N.R., Barmby, P., et al. 2010, *ApJ*, 709, 120
- Monson, A., Freedman, W.L., Madore, B.F., et al. 2012, *ApJ*, 759, 146
- Persson, S.E., Madore, B.F., Krzeminski, W., et al. 2012, *AJ*, 128, 2239
- Scowcroft, V., Freedman, W.L., Madore, B.F., et al. 2011, *ApJ*, 743, 76
- Sollima, A., Cacciari, C., & Valenti, E. 2006, *MNRAS*, 372, 1675
- Wright, E.L., Eisenhardt, P.R.M., Mainzer, A.K., et al. 2010, *AJ*, 140, 1868
- Yuan,H.B., Liu, X.W., & Xiang, M.S. 2013, *MNRAS*, 430, 2188

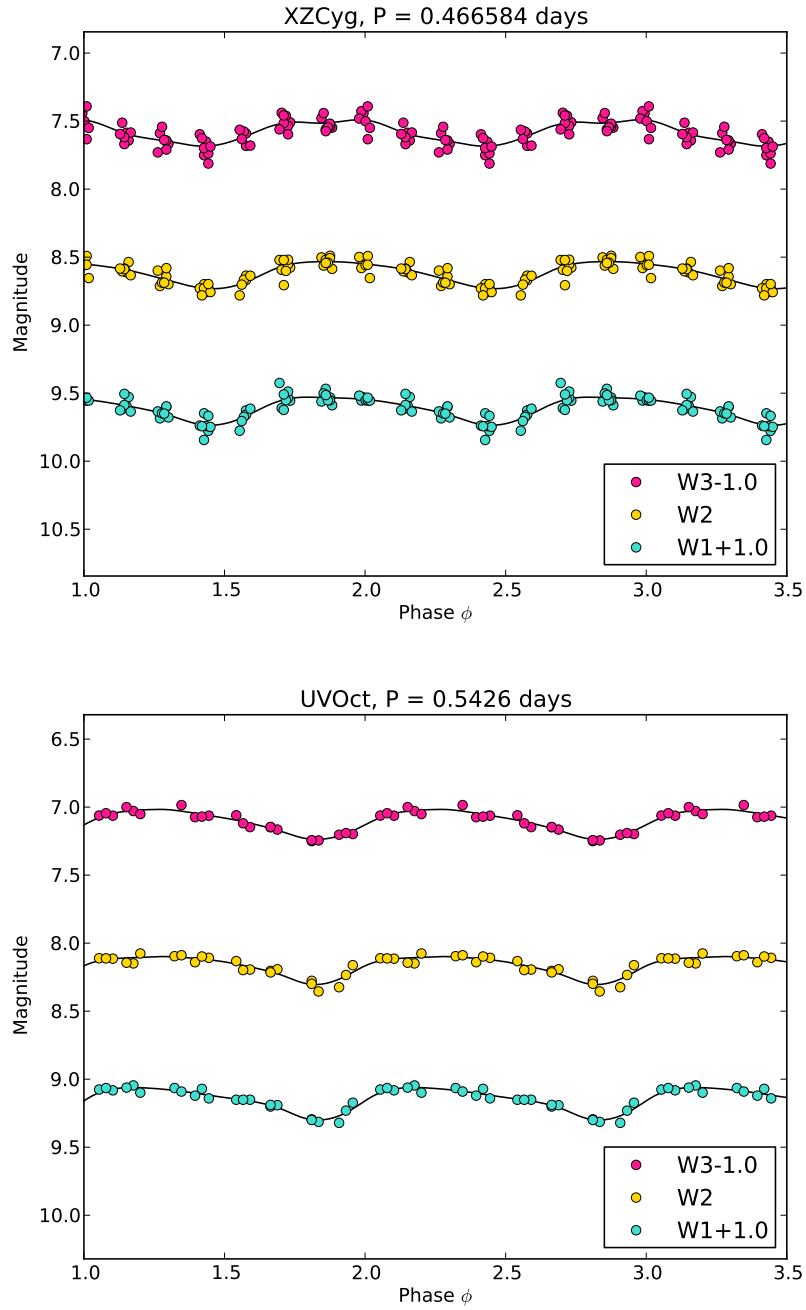


Fig. 1.— WISE Mid-Infrared light curves for XZ Cyg (upper panel) and UV Oct (lower panel) phase-folded over two and a half cycles using the periods given in the titles. GLOESS fits are shown as solid black lines.

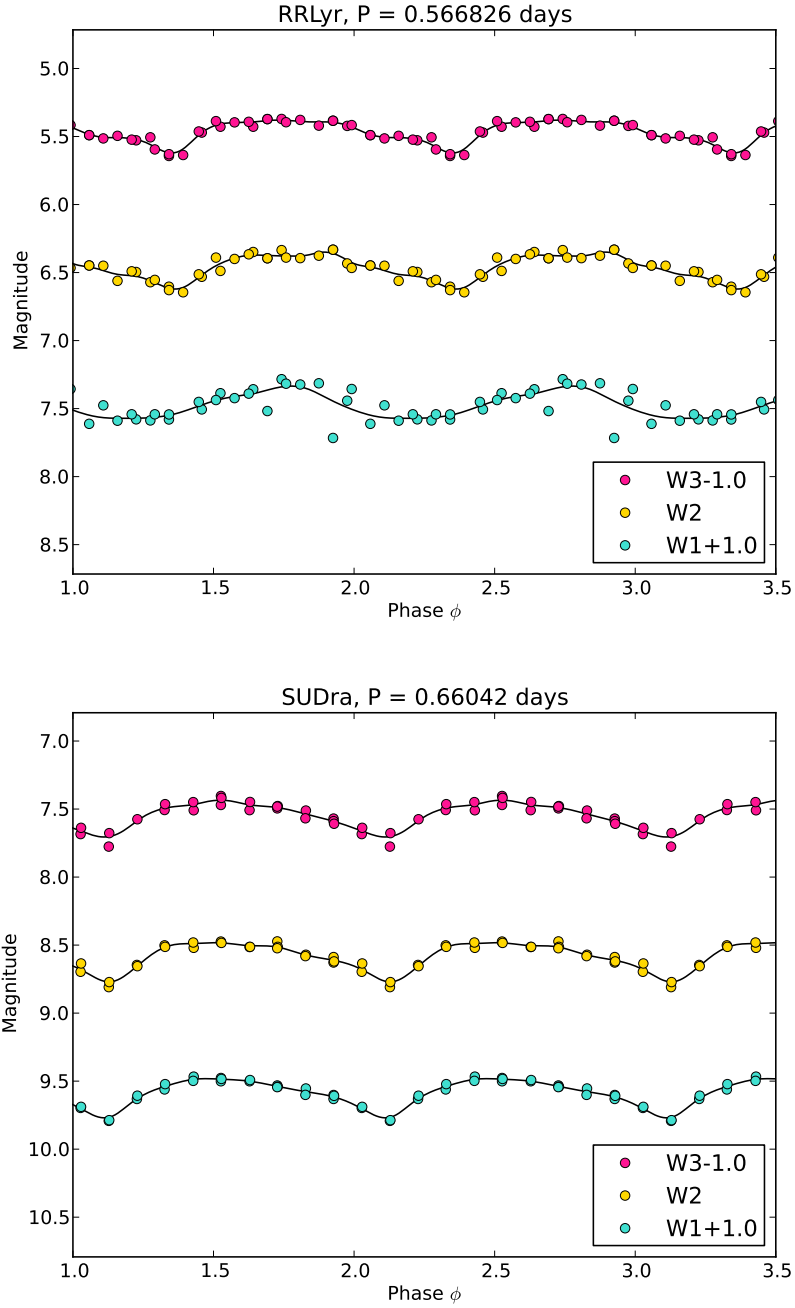


Fig. 2.— WISE Mid-Infrared light curves for RR Lyr (upper panel) and SU Dra (lower panel) phase-folded over two and a half cycles using the periods given in the titles. GLOESS fits are shown as solid black lines.

RR Lyrae PL Relations

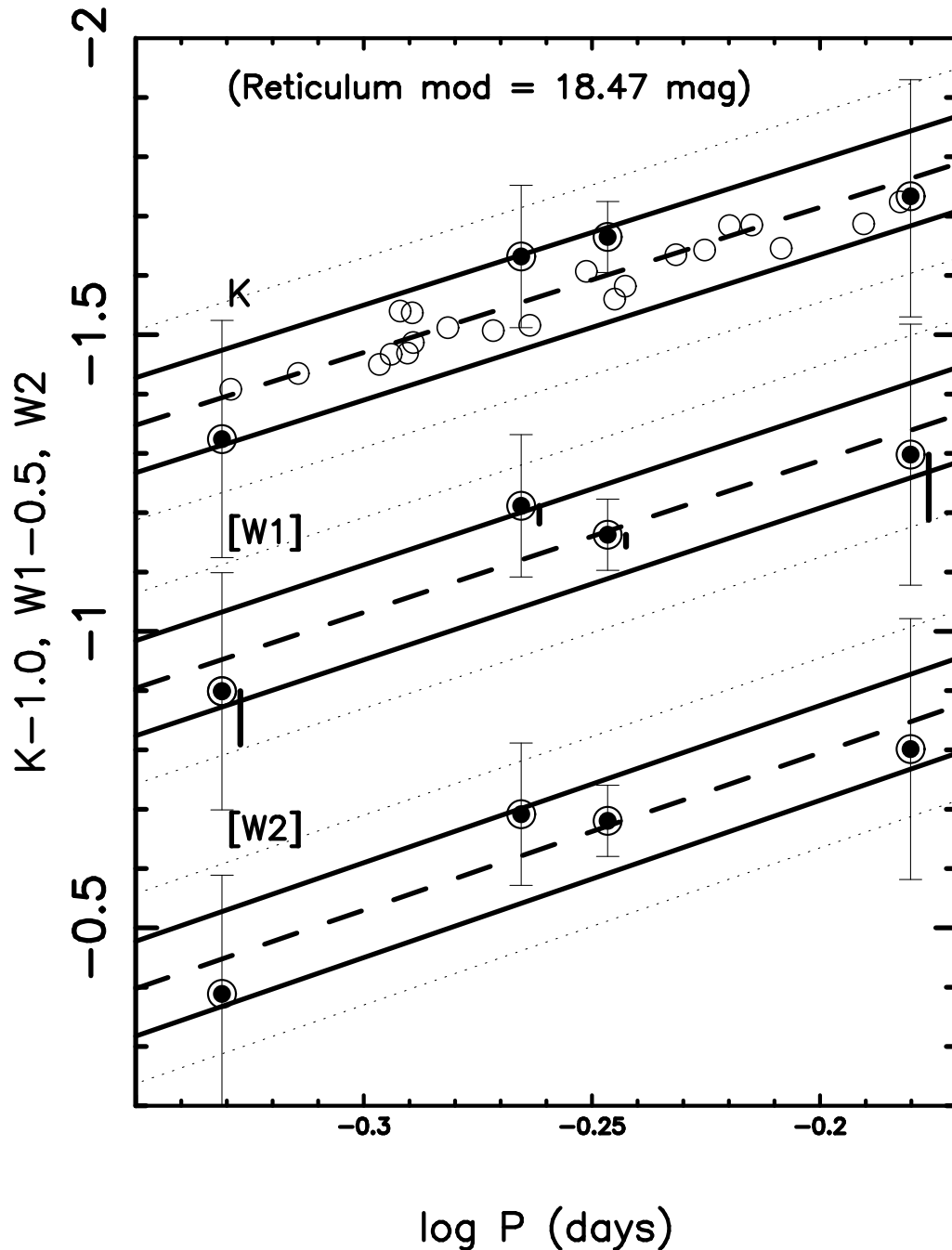


Fig. 3.— RR Lyrae PL relations in the K-band (top) and the two WISE bands [W1] (middle and [W2] bottom). The K-band relation also contains data from Dall’Ora et al. (2004) for the LMC globular cluster, Reticulum, shifted by 18.47 mag. (This distance modulus shift is remarkably close to the independently-determined true modulus of 18.48 mag recently reported by Monson et al. 2012 for the LMC Cepheid mid-infrared distance modulus.) The Reticulum data are shown only for the RRab (fundamental) pulsators, and are presented here to illustrate that they are consistent in slope and scatter in comparison with the Galactic calibration. A detailed discussion of Reticulum will be given in a forthcoming paper (Monson et al. 2013). The solid lines flanking each of the fitted PL relations are each separated by two sigma from their respective ridge lines. Despite the small numbers of stars represented here the full width of the PL relation in each of the bands is well defined. The solid vertical lines to the right of each of the [W1] data points

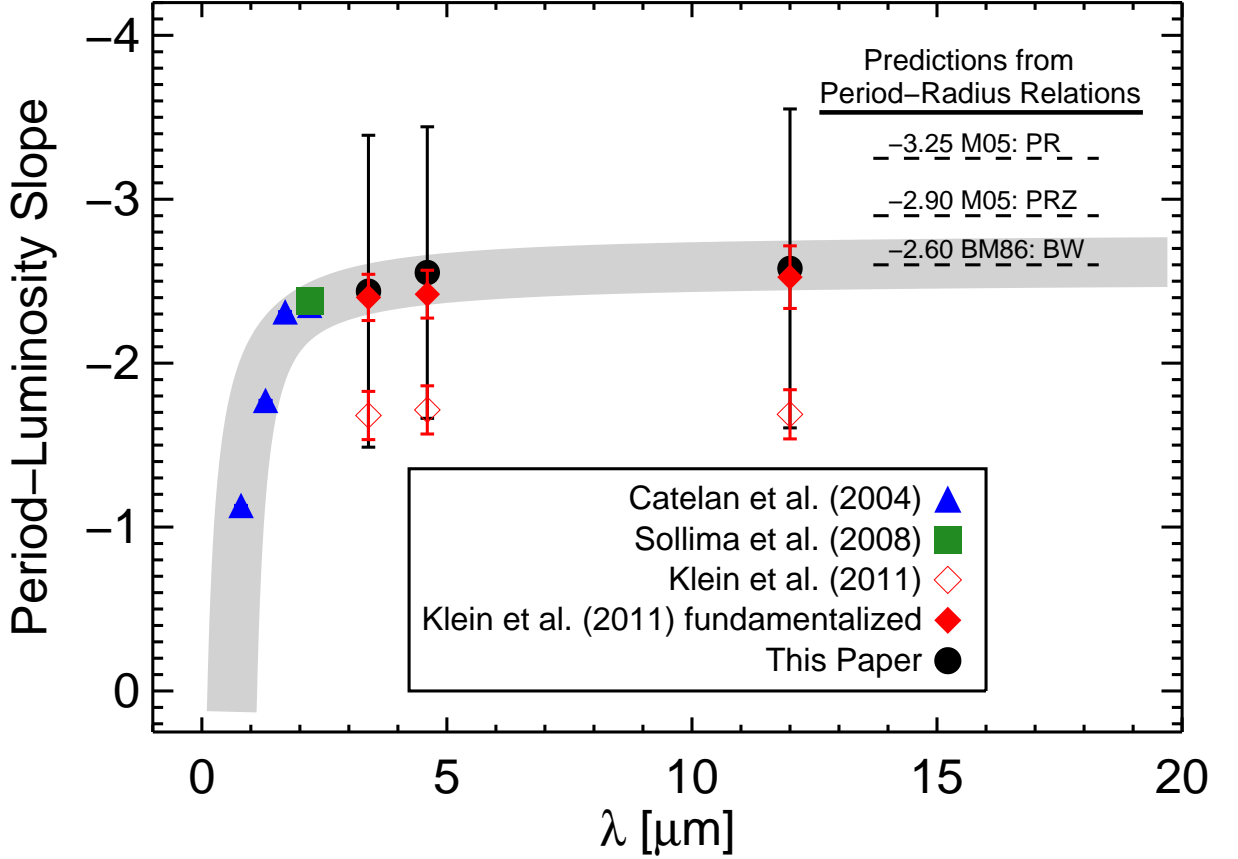


Fig. 4.— The expected monotonic increase of the slope of the RR Lyrae Period-Luminosity relation as a function of increasing wavelength. The asymptotic behavior of the slope, approaching a value of about -2.6 indicates that the PL relation is converging on the Period-Radius relation, as theory would predict, given that the sensitivity of the surface brightness to temperature rapidly drops as one progressively moves into the infrared. The open diamonds are the slopes published by Klein et al. (2011); the filled (red) diamonds indicate the “fundamentalized” slopes (where we have corrected the periods of the overtone pulsators to their corresponding fundamental periods by adding 0.127 to the log of their observed periods, as in Dall’Ora et al. 2004), based on the data published by Klein et al. (2011) and re-fit for this paper. The optical and near-infrared PL relation slopes are from Catelan, Pritzl & Smith (2004), Benedict et al. (2011) and Sollima, Cacciari & Valenti al. (2006), while the mid-IR slopes are from this study. The equivalent slopes derived from Period-Radius relations are from Burki & Meylan (1986; BM86) and Marconi et al. (2005; M05).

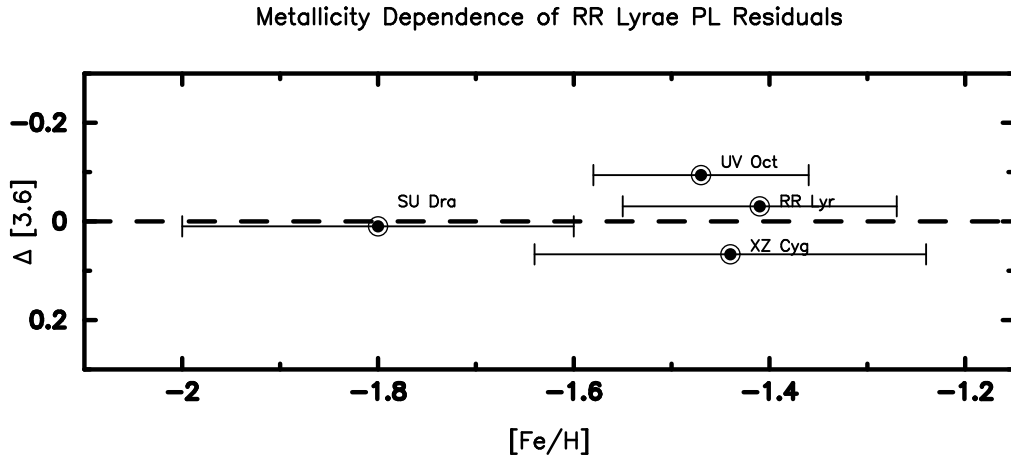


Fig. 5.— Mid-Infrared [W1] ($3.4 \mu\text{m}$) deviations from the mean Period-Luminosity relation as a function of metallicity. The currently available sample is small, and the metallicity range is limited. No obvious correlation is seen.

Table 1. Mid-Infrared (WISE) Magnitudes for Galactic RR Lyrae Variables

Name	XZ Cyg	UV Oct	RR Lyr	SU Dra
$\log(P)$	-0.33107	-0.26552	-0.24655	-0.18018
parallax (mas)	1.67 ± 0.17	1.71 ± 0.10	3.77 ± 0.13	1.42 ± 0.16
A_V^a	0.30	0.28	0.13	0.03
A_{W1}	0.020	0.018	0.008	0.002
A_{W2}	0.016	0.015	0.007	0.002
A_{W3}	0.002	0.001	0.001	0.000
LKH Corr.	-0.09	-0.03	-0.02	-0.11
$(m - M)_o$	8.98	8.87	7.14	9.35
$m[W1]$	8.610	8.156	6.469	8.584
$\sigma[W1]$	0.010	0.017	0.017	0.019
Ampl [W1]	0.21	0.24	0.24	0.29
$m[W2]$	8.616	8.172	6.456	8.580
$\sigma[W2]$	0.010	0.014	0.017	0.019
Ampl [W2]	0.20	0.21	0.27	0.29
$m[W3]$	8.579	8.110	6.460	8.543
$\sigma[W3]$	0.010	0.016	0.015	0.018
Ampl [W3]	0.19	0.22	0.24	0.27
$M[W1]$	-0.39 (0.23)	-0.73 (0.13)	-0.68 (0.08)	-0.77 (0.26)
$M[W2]$	-0.38 (0.23)	-0.71 (0.13)	-0.69 (0.08)	-0.77 (0.26)
$M[W3]$	-0.40 (0.23)	-0.76 (0.13)	-0.68 (0.08)	-0.81 (0.26)

^a Benedict et al. (2011), where $A_{band}/E(B-V) = 0.20, 0.16, 0.03$ for W1, W2 and W3, respectively.

Table 2. WISE Observations of RR Lyrae

MJD(2,400,000.+)	3.4 μm	err	4.6 μm	err	12 μm	err
55312.047509	6.612	0.019	6.448	0.022	6.490	0.014
55312.179813	6.542	0.034	6.554	0.019	6.595	0.019
55312.312118	6.387	0.031	6.488	0.020	6.428	0.013
55312.378206	6.358	0.049	6.349	0.021	6.428	0.019
55312.444422	6.317	0.030	6.390	0.019	6.395	0.014
55312.510510	6.314	0.032	6.376	0.018	6.420	0.019
55312.576726	6.356	0.034	6.466	0.017	6.416	0.016
55312.642814	6.476	0.031	6.450	0.021	6.514	0.016
55312.709030	6.579	0.026	6.496	0.021	6.528	0.016
55312.775119	6.580	0.041	6.604	0.019	6.643	0.017
55312.775246	6.543	0.029	6.629	0.020	6.630	0.020
55312.841334	6.506	0.028	6.531	0.019	6.471	0.018
55312.907423	6.423	0.032	6.400	0.016	6.396	0.013
55312.973639	6.518	0.04	6.395	0.018	6.372	0.017
55313.039855	6.323	0.037	6.394	0.020	6.378	0.018
55313.105943	6.716	0.04	6.332	0.017	6.384	0.019
55313.238247	6.589	0.030	6.561	0.017	6.495	0.016
55313.304463	6.587	0.029	6.571	0.015	6.506	0.016
55313.436767	6.437	0.044	6.390	0.018	6.387	0.014
55313.502856	6.390	0.037	6.366	0.013	6.392	0.014
55313.569072	6.284	0.034	6.335	0.020	6.371	0.016
55313.701376	6.442	0.030	6.433	0.028	6.422	0.014
55313.833680	6.542	0.032	6.491	0.022	6.523	0.017
55321.904496	6.451	0.038	6.513	0.018	6.463	0.016

Table 3. WISE Observations of SU Draconis

MJD(2,400,000.+)	3.4 μm	err	4.6 μm	err	12 μm	err
55315.013213	8.561	0.019	8.502	0.017	8.507	0.037
55315.145517	8.501	0.021	8.474	0.022	8.470	0.043
55315.145644	8.477	0.022	8.479	0.021	8.404	0.039
55315.277821	8.544	0.023	8.523	0.019	8.482	0.040
55315.277949	8.532	0.022	8.473	0.023	8.495	0.040
55315.344037	8.601	0.017	8.581	0.013	8.568	0.040
55315.410125	8.631	0.022	8.628	0.019	8.570	0.044
55315.410253	8.602	0.021	8.588	0.017	8.589	0.046
55315.476341	8.697	0.020	8.696	0.017	8.684	0.046
55315.542559	8.792	0.021	8.809	0.017	8.776	0.052
55315.608647	8.631	0.017	8.646	0.019
55315.674863	8.522	0.021	8.513	0.016	8.464	0.043
55315.740952	8.498	0.017	8.481	0.017	8.449	0.043
55315.807167	8.484	0.025	8.484	0.020	8.418	0.037
55315.873256	8.501	0.020	8.514	0.019	8.508	0.039
55315.939472	8.541	0.020	8.513	0.020	8.478	0.040
55316.005560	8.554	0.018	8.571	0.016	8.511	0.040
55316.071776	8.608	0.021	8.620	0.019	8.608	0.045
55316.137864	8.689	0.021	8.635	0.019	8.638	0.043
55316.204080	8.787	0.018	8.772	0.024	8.677	0.043
55316.270169	8.607	0.016	8.655	0.018	8.575	0.042
55316.402473	8.467	0.019	8.520	0.022	8.509	0.045
55316.534777	8.492	0.026	8.513	0.020	8.448	0.039

Table 4. WISE Observations of UV Oct

MJD(2,400,000.+)	3.4 μm	err	4.6 μm	err	12 μm	err
55270.919633	8.082	0.025	8.114	0.020	8.063	0.031
55271.052065	8.091	0.021	8.089	0.015	7.985	0.029
55271.184369	8.151	0.019	8.194	0.020	8.147	0.032
55271.316673	8.314	0.016	8.355	0.018	8.245	0.032
55271.382761	8.173	0.028	8.162	0.019	8.198	0.032
55271.448977	8.065	0.019	8.112	0.017	8.045	0.030
55271.515192	8.099	0.020	8.076	0.016	8.051	0.029
55271.581281	8.065	0.018	8.096	0.016
55271.647496	8.141	0.019	8.108	0.021	8.063	0.030
55271.713585	8.151	0.022	8.198	0.019	8.119	0.034
55271.779800	8.191	0.020	8.192	0.022	8.165	0.030
55271.845888	8.300	0.022	8.299	0.020	8.243	0.034
55271.846016	8.295	0.022	8.277	0.022	8.250	0.032
55271.912104	8.231	0.019	8.234	0.017	8.191	0.032
55271.978320	8.076	0.026	8.111	0.016	8.062	0.028
55272.044408	8.046	0.018	8.149	0.017	8.029	0.029
55272.176712	8.071	0.021	8.098	0.019	8.070	0.033
55272.242928	8.151	0.017	8.132	0.013	8.060	0.029
55272.309016	8.201	0.022	8.204	0.019	8.148	0.033
55272.309144	8.189	0.022	8.215	0.022	8.146	0.031
55272.441448	8.321	0.021	8.324	0.020	8.203	0.033
55272.573751	8.062	0.023	8.144	0.028	8.000	0.030
55272.706056	8.121	0.017	8.140	0.013	8.074	0.029

Table 5. WISE Observations of XZ Cyg

MJD(2,400,000.+)	3.4 μm	err	4.6 μm	err	12 μm	err
55334.008212	8.589	0.016	8.586	0.017	8.548	0.037
55334.140516	8.635	0.016	8.633	0.017	8.584	0.040
55334.272820	8.748	0.019	8.757	0.017	8.687	0.048
55334.339035	8.614	0.018	8.637	0.021	8.680	0.049
55334.405124	8.555	0.019	8.577	0.018	8.509	0.041
55334.471212	8.552	0.028	8.508	0.020	8.519	0.039
55334.471339	8.532	0.018	8.490	0.021	8.540	0.048
55334.537428	8.554	0.019	8.654	0.020	8.550	0.040
55334.603643	8.528	0.025	8.536	0.015	8.642	0.040
55334.669732	8.678	0.020	8.699	0.020	8.667	0.046
55334.735820	8.777	0.023	8.725	0.021	8.738	0.044
55334.735947	8.667	0.023	8.698	0.015	8.812	0.046
55334.868124	8.536	0.023	8.553	0.022	8.536	0.038
55334.868251	8.488	0.026	8.519	0.015	8.597	0.045
55334.934340	8.553	0.019	8.541	0.017	8.546	0.044
55335.000428	8.533	0.027	8.556	0.020	8.392	0.035
55335.000555	8.554	0.022	8.492	0.020	8.633	0.046
55335.066644	8.593	0.019	8.612	0.018	8.586	0.047
55335.132732	8.602	0.026	8.643	0.020	8.642	0.041
55335.132859	8.597	0.019	8.581	0.018	8.709	0.047
55335.198947	8.742	0.017	8.757	0.021	8.651	0.044
55335.265036	8.627	0.021	8.669	0.016	8.591	0.039
55335.265163	8.658	0.023	8.636	0.021	8.682	0.044
55335.331251	8.552	0.017	8.601	0.021	8.461	0.041
55335.397340	8.468	0.019	8.520	0.016	8.560	0.039
55335.397467	8.514	0.024	8.543	0.020	8.574	0.044

Table 5—Continued

MJD(2,400,000.+)	3.4 μm	err	4.6 μm	err	12 μm	err
55335.463555	8.552	0.017	8.559	0.019	8.501	0.043
55335.529644	8.587	0.019	8.588	0.016	8.619	0.040
55335.529771	8.505	0.021	8.584	0.021	8.669	0.045
55335.595859	8.650	0.017	8.688	0.020	8.639	0.047
55335.661948	8.844	0.022	8.729	0.019	8.698	0.046
55335.662075	8.648	0.021	8.699	0.023	8.751	0.050
55335.728163	8.674	0.017	8.666	0.019	8.577	0.044
55335.794252	8.623	0.023	8.521	0.019	8.459	0.040
55335.794379	8.509	0.023	8.706	0.029	8.514	0.043
55335.860467	8.502	0.018	8.562	0.017	8.441	0.040
55335.926556	8.531	0.021	8.546	0.020	8.442	0.040
55335.992771	8.617	0.019	8.604	0.017	8.512	0.040
55336.058860	8.648	0.021	8.687	0.020	8.542	0.042
55336.125075	8.743	0.020	8.781	0.026	8.626	0.041
55336.191164	8.705	0.022	8.702	0.020	8.632	0.045
55336.257379	8.610	0.019	8.593	0.024	8.439	0.036
55336.323468	8.561	0.021	8.502	0.019	8.478	0.039
55336.389683	8.554	0.024	8.580	0.026	8.427	0.038
55336.455772	8.626	0.022	8.584	0.017	8.595	0.048
55336.521985	8.685	0.017	8.712	0.014	8.589	0.039
55336.588074	8.738	0.021	8.729	0.023	8.597	0.044
55336.654289	8.776	0.018	8.781	0.014	8.564	0.040
55336.720377	8.425	0.021	8.521	0.017	8.561	0.039
55336.852681	8.518	0.018	8.499	0.016	8.481	0.038
55336.984985	8.634	0.019	8.599	0.017	8.730	0.046